Emission Processes in YVO_4:Eu Nanoparticles

Arnaud Huignard,† Valérie Buissette,† Anne-Christine Franville,‡ Thierry Gacoin,† and Jean-Pierre Boilot*,†

Groupe de Chimie du Solide, Laboratoire de Physique de la Matière Condensée, CNRS UMR 7643, École Polytechnique, 91128 Palaiseau Cedex, and Laboratoire des Matériaux Inorganiques, 24 Avenue des Landais, 63177 Aubière Cedex, France

Received: January 28, 2003; In Final Form: May 7, 2003

The luminescence properties of colloidal YVO_4:Eu nanoparticles (8 nm in diameter) are investigated and compared to those of the bulk materials. The emission quantum yield of nanoparticles is improved after the transfer of the colloidal particles into D_2O, showing that surface OH groups act as efficient quenchers of the Eu^{3+} emission. The growth of a silicate shell around the nanoparticles decreases the optimum europium concentration, showing that energy transfers within the nanoparticles are limited by the quenching of the excited states of the vanadate groups. Nanoparticles also exhibit structural distortions directly related to the small size of the particles. No clear evidence is found concerning the influence of these distortions on the energy-transfer processes, since the improvement of the emission properties observed after thermal annealing of both crude and silicated powders seems to result mainly from the elimination of Eu^{3+} and vanadate quenchers from the surface. This latter effect is greatly enhanced in the presence of the silicate shell compared to bare particles.

1. Introduction

Advanced technologies for the design of new devices such as flat panel displays, integrated optics, and any development associated with the new GaN technology provide new motivations for the research of luminescent materials with optimized properties.[1] One aspect of this work concerns the investigation of the emission properties of materials with a grain size in the nanometer range. Only a few studies have been performed yet, mostly because the conventional ceramic processing techniques do not allow such small grain sizes to be obtained. Nevertheless, important improvements have been achieved in the last 10 years in the low-temperature chemical processing of materials. Especially, colloid chemistry has been shown to be a very powerful technique to prepare well-dispersed nanoparticles with a controlled size, shape, and surface state. A now famous example is the case of II−VI semiconductors, for which a huge amount of work has finally shown the possibility to synthesize nanoparticles with a very narrow size distribution and a luminescence quantum yield up to 60%.[2] Now, the extension of this research to other highly luminescent compounds such as the rare-earth-doped oxides[3] requires the chemical processes to be adapted to obtain nanocrystals with a good crystallinity and controlled chemical composition, size, and surface state. Up to now, several systems emitting in the visible range have been synthesized (Y_2O_3:Eu,Tb,[4] Y_2SiO_5:Eu,[5] $Sr_5(PO4)_3Cl$:Eu[6]), most of them being agglomerated powders of nanoparticles obtained after high-temperature treatments (calcination, combustion, laser ablation). Fewer studies have concerned the colloidal synthesis of well-dispersed nanoparticles through colloidal routes: YVO_4:Eu,Sm,Dy,[7,8] $LaPO_4$:Eu,Ce,Tb,[9] $CePO_4$:Tb,[10] and LaF_3:Er,Nd,Ho.[11]

In this paper, we discuss in detail the emission properties of YVO_4:Eu nanoparticles for which the synthesis has already been studied in our group and the group of Haase.[7,8] Especially, our aim is to have a better understanding of the chemical or structural parameters that are involved in the radiative or nonradiative relaxation of the excited states after absorption of the UV light. This research is achieved through the study of the influence of different chemical and thermal treatments on the emission characteristics of the nanoparticles such as their emission quantum yield and lifetime.

2. Experimental Section

Synthesis of $Y_{1-x}Eu_xVO_4$ Colloids.[7] The whole process is carried out in water. A 0.1 mol·L^{-1} solution of $(Y,Eu)(NO_3)_3$ (10 mL, 1 mmol) is mixed with a 0.1 mol·L^{-1} solution of sodium citrate (7.5 mL, 0.75 mmol). This leads to the formation of a white precipitate of lanthanide citrate, which is completely dissolved at room temperature by the addition of a 0.1 mol·L^{-1} solution of Na_3VO_4 (7.5 mL, 0.75 mmol), whose pH is fixed at 12.5 using sodium hydroxide. The clear and colorless resulting mixture, whose pH is 8.4, is subsequently heated at 60 °C for 30 min. Finally, the solution is cooled and dialyzed against water. The concentration of the colloidal solutions obtained at this step is 10^{-2} M. Powders of nanocrystals are obtained by eliminating water via a rotary evaporator under mild conditions (40 °C under vacuum). These powders can then be dispersed in water, leading to transparent colloidal solutions up to 400 g·L^{-1}. The average size of the particles, as determined by transmission electron microscopy, is 8 nm with a standard deviation of 3.1. The homogeneous incorporation of Eu^{3+} ions inside the YVO_4 zircon-type structure has been previously checked using X-ray diffraction experiments on $Y_{1-x}Eu_xVO_4$ nanoparticles.[7] In all the composition range (from $x = 0$ to $x = 1$), the evolution of the volume of the unit cell was linear, showing the existence of a solid solution.

* To whom correspondence should be addressed. E-mail: jean-pierre.boilot@polytechnique.fr.
† École Polytechnique.
‡ Laboratoire des Matériaux Inorganiques.

10.1021/jp0342226 CCC: $25.00
Published on Web 06/14/2003

Silica Coating of the Particles. The nanoparticles are coated by a functionalized alkoxide following a process adapted from the work of Philipse in the case of bohemite nanoparticles.[12,13] In the first step, 50 mL of an aqueous solution of sodium silicate (3% SiO_2, 1% Na_2O) is added to a colloidal solution of YVO_4 nanoparticles ($[YVO_4] = 0.05$ mol·L^{-1}). The resulting solution is left under stirring at ambient temperature for 18 h, and then dialyzed against water for 48 h. The colloid is then concentrated down to 100 mL and added dropwise to 300 mL of a solution of ethanol containing 5 equiv of (3-methacryloxylpropyl)-trimethoxysilane. This mixture is then refluxed for 24 h and transferred to 400 mL of 1-propanol so that water can be further removed by azeotropic distillation. The grafted colloids are then concentrated up to 0.5 mol·L^{-1}.

Characterizations. Emission and excitation spectra as well as lifetime measurements are recorded on a commercial Hitachi F-4500 spectrofluorometer. The quantum yields of the colloidal solutions are determined by comparing their integrated emission intensity with the emission from a Rhodamine 6G solution in ethanol having the same optical density (OD < 0.3) and excited at the same wavelength (280 nm). In the case of powders, quantum yields are determined by comparing the integrated emission of a given surface of compacted powders with the emission of a powder of destabilized colloids whose quantum yield was determined as previously described.

X-ray diffraction (XRD) studies are performed on the powders of nanocrystals using a Philips X-Pert diffractometer with Cu Kα radiation ($\lambda = 1.54$ Å). The coherence length is determined from the full width at half-maximum of the diffraction peaks using Sherrer's law. It approximately corresponds to the average size of crystallites, i.e., to the size of particles in the case of nonaggregated crystalline nanoparticles. Size-strain analysis of X-ray diagrams is performed using the Williamson−Hall procedure.[14]

3. Results and Discussion

Luminescence of the Crude Particles (cp) and Comparison with the Bulk Material. As reported in previous works,[8] the absorption of UV light by the vanadate ions in the nanoparticles does not significantly differ from that by isolated vanadate ions dissolved in solution. The comparison with the absorption in the bulk YVO_4:Eu is made difficult since precise measurements are limited by saturation effects. Nevertheless, a recent study performed on thin films enables confirmation that the absorption spectrum of vanadates in our colloids is not much different from the absorption spectrum of highly crystalline YVO_4 thin films (Figure 1).[15]

The emission spectra of both bulk and colloidal YVO_4:Eu (5% Eu^{3+}) samples are presented in Figure 2. The spectra are dominated by the emission from the europium ions, and mainly the $^5D_0-^7F_{2,4}$ forced electric-dipole transitions for which high intensities are a consequence of the absence of an inversion symmetry at the Eu^{3+} lattice site (D_{2d} symmetry). Other contributions of weaker importance are the $^5D_0-^7F_{1,3}$ magnetic dipole transitions. In both samples, all the main transitions are observed with the same average energy and almost the same relative intensity. Especially, the ratios of the $^5D_0-^7F_2$ and $^5D_0-^7F_1$ integrated transition intensities are nearly the same in both samples (equal to 9.3), showing that the environment of the Eu^{3+} ion is almost the same in the nanoparticles and in the bulk material.

The excitation spectrum corresponding to the europium emission of nanoparticles (Figure 1) fits well with the absorption spectrum from the vanadate ions, which confirms that the emission occurs after energy transfer from the excited vanadate to the europium ions. The mechanism of this transfer has been the subject of many investigations, and is now well-known to occur after a thermally activated energy migration through the vanadate sublattice.[16] The whole emission process can then be briefly summarized as presented in Scheme 1 (pathways 1−4).[17]

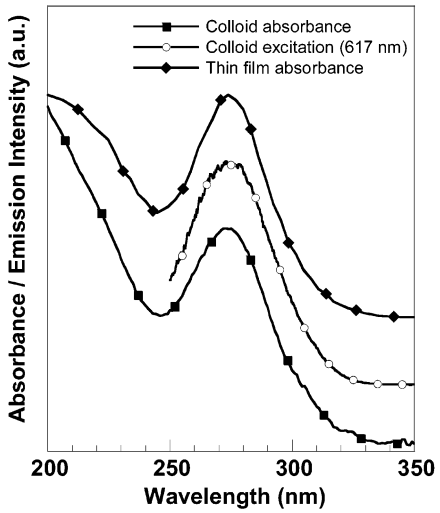

Figure 1. UV absorbance of vanadate groups in YVO_4:Eu colloids. The curve for thin films is adapted from ref 15 (Copyright 2002 American Chemical Society). The excitation spectrum shows that the europium emission of nanoparticles implies an energy-transfer mechanism from the excited vanadate groups to europium ions.

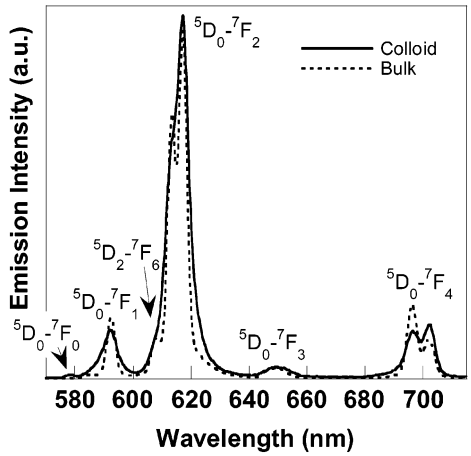

Figure 2. Emission spectra of both bulk (dashed line) and colloidal (full line) YVO_4:Eu (5% Eu^{3+}) samples.

However, a major difference between the emission behavior of the colloid compared to the bulk materials is observed when the luminescence quantum yield is plotted as a function of the europium content (Figure 3, bulk and cp curves). In the bulk material, a clear optimum of the luminescence quantum yield (70%) is obtained for a europium concentration of 5%.[18] In the case of colloidal particles, this optimum is no more well defined, and occurs in the 15−30% europium content range, while the maximum efficiency does not go beyond 20%. Concerning the $^5D_0$ luminescence lifetime, a decrease is observed in both cases for increasing Eu^{3+} content. Nevertheless, the lifetime measured for the colloidal particles is always much higher than in the bulk material (Figure 4).

Surface Effects: Quenching of the Europium Emission. As discussed in a previous paper,[2] an important source of luminescence quenching in small particles is the surface, where the coordination of the atoms differs from that in the bulk and

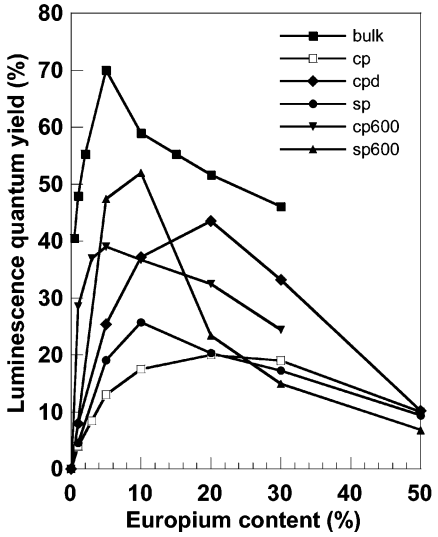

Figure 3. Evolution of the luminescence quantum yield as a function of the europium content for $Y_{1-x}VO_4:Eu_x$ nanoparticles after different chemical and thermal treatments (cp, crude nanoparticles in water; sp, silica-capped nanoparticles in ethanol; cpd, crude nanoparticles in deuterated water; cp600, powder of crude particles annealed at 600 °C; sp600, powder of silica-capped particles annealed at 600 °C; bulk, YVO_4:Eu micronic crystalline powder[18]).

SCHEME 1 . Representation of Energy-Transfer Pathways (1−8) Leading to Radiative Eu Emission ($h\nu_{em}$) or Nonradiative Quenching (Q) after UV Light Absorption by Vanadate Groups ($h\nu_{ex}$) in YVO_4:Eu Samples

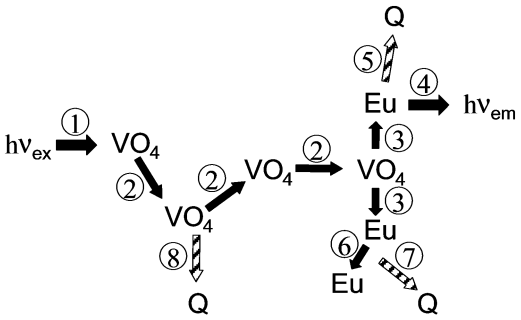

where different chemical species can be adsorbed. Considering that our synthesis process is achieved in water, the surface of the nanocrystals can be covered by a large number of hydroxyl species (yttrium or europium hydroxides, bending vanadates, or adsorbed water molecules), as well as citrate complexes. Hydroxyl groups are well-known to quench the emission from Eu^{3+} (pathway 5 in Scheme 1) since the energy of the $^5D_0-{}^7F_6$ transition of relaxation nearly corresponds to the third harmonic of the vibration mode of the OH oscillator. This effect is indeed evidenced by the transfer of the nanoparticles into D_2O. Since the vibrational energy of the OD group is lower than that of the OH group, the energy of the $^5D_0-{}^7F_6$ transition now corresponds to the fifth harmonic of the vibration mode of the OD oscillator. This makes the probability of relaxation about 200 times lower than in the presence of OH groups.[19] Figures 3 and 4 (cpd curve) show the evolution of the emission properties of the colloids after their transfer into deuterated water. A clear increase of both the luminescence quantum yield and the emission lifetime is observed, which confirms that surface OH groups are efficient quenchers of the excited europium ions. Nevertheless, if the transfer into D_2O has multiplied the emission yield by a factor of about 2, it also clearly appears that this effect is nearly independent of the europium content so that the shape of the curve of the quantum yield versus the europium content does not change. Considering this, the reasons why the evolution of the emission quantum yield of nanoparticles, as a function of the europium content, markedly differs from that of bulk materials have to be found in the energy migration processes which occur between the absorption of a photon by vanadate groups and the final transfer of the excitation to Eu^{3+} ions.

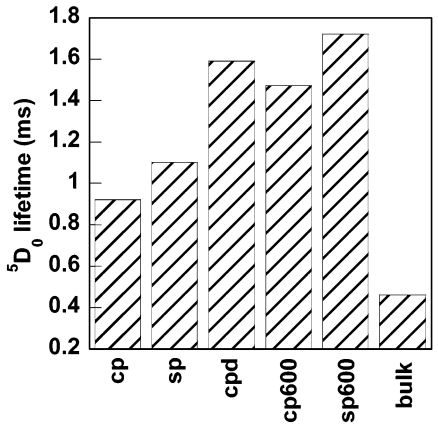

Figure 4. Evolution of the $^5D_0$ luminescence lifetime for YVO_4:Eu (5% Eu^{3+}) samples after a chemical or a thermal treatment. All the measured lifetimes were single exponential (cp, crude nanoparticles in water; sp, silica-capped nanoparticles in ethanol; cpd, crude nanoparticles in deuterated water; cp600, powder of crude particles annealed at 600 °C; sp600, powder of silica-capped particles annealed at 600 °C, bulk, YVO_4:Eu micronic crystalline powder[18]).

Surface Effects: Alteration of the $VO_4^{3-}-VO_4^{3-}$ Energy Transfers. It is indeed well-known that the optimum of the europium concentration results from two competitive effects: on one hand, an increase of the europium concentration improves the probability of the energy transfers to europium ions (pathway 3, Scheme 1), and thus radiative recombination. But on the other hand, there is also an increase of the probability of energy transfer between europium ions (pathway 6, Scheme 1) which increases the efficiency of the excitation capture by nonradiative recombination centers (concentration quenching, pathway 7, Scheme 1). This behavior is well-known for bulk phosphors with luminescent ions as activators of the luminescence, but the observation of a high luminescence quantum yield for a quite small europium content in the case of the $Y_{1-x}VO_4:Eu_x$ bulk has to be related to the very efficient transfer of the energy through adjacent vanadate species, until the excitation reaches a europium ion.

Considering the general Scheme 1, a possible reason for the alteration of the energy transfers in nanoparticles may be found in nonradiative processes leading to the deexcitation of the vanadate species (pathway 8, Scheme 1). This effect is expected because the average migration distance of the exciton in the bulk material is about 9 nm,[16] which nearly corresponds to the size of our nanoparticles. Surface quenching of the excitation is thus highly probable in this size range. This idea is supported by the investigation of the luminescence efficiency of particles covered with a silicate shell (see the Experimental Section). In this case, a clear shift of the optimum europium content is observed (sp curve, Figure 3), which attests the finding that the coverage of the particles by a silicate shell improves the energy migration. This passivation only concerns the vanadate species, since the global emission yield is still limited by OH quenching, and the $^5D_0$ lifetime of the europium remains almost unchanged (Figure 4). Therefore, these experiments show that the surface of the crude particles presents

efficient quenching centers for the deexcitation of the vanadates. This provides experimental evidence for the conclusions of Riwotzki and Haase in their study of the temperature dependence of the vanadate emission in $YP_{0.95}V_{0.05}O_4$:Eu and YVO_4:Eu nanoparticles.[20] The chemical nature of the passivation of the surface by the silicate shell is not clear yet, but may be attributed to the formation of V−O−Si bonds, which could be less active quenchers than bending V−OH or $V-O^-$ groups.

Structural Distortions in Nanoparticles: Origin and Thermal Evolution. Another possible reason for the alteration of the energy transfers may be found in lattice distortions within the nanocrystals. As discussed by Van Uitert[21] and Blasse,[22] almost all the energy transfers which occur after the absorption of light ($VO_4^{3-}-VO_4^{3-}$, $VO_4^{3}-Eu^{3+}$, and $Eu^{3+}-VO_4^{3-}-Eu^{3+}$) take place through exchange interactions. These transfers are all the more favored when the wave function overlaps are efficient. This explains the high luminescence of bulk YVO_4:Eu, since the V−O−Y angle of 170° makes the σ bonding overlap almost optimum. This implies that distortions of the crystalline lattice may alter the energy migration processes through decreasing wave function overlaps.

Structural distortions within the nanocrystals are found by considering the width of the emission bands, which is larger in the nanoparticles than in the bulk materials. Although transitions within f electrons of rare earth ions are not very sensitive to a crystal field, enlargements of transitions are commonly observed in the case of these ions with a distribution of environments such as in amorphous host matrixes.[23] In our case, this distribution seems to occur from slight distortions of the crystalline lattice more than from a difference of local chemical environments since the ratio of the $^5D_0-^7F_2$ and $^5D_0-^7F_1$ integrated transition intensities is similar to that of the bulk. Such distortions are also evidenced considering the relative intensity of the two main contributions of the $^5D_0-^7F_4$ transitions, $^5D_0(A_1)-^7F_4(B_2)$ and $^5D_0(A_1)-^7F_4(E^{(1)})$, which is different from that of the bulk material (Figure 2). The oscillator strength of these transitions is all the more affected by distortions that obey selection rules for electromagnetic transitions in dodecahedral symmetry.[24]

Once these distortions have been evidenced, the question is now to know whether they have an impact on the energy transfers involved in the emission processes. Two main explanations can be given for the presence of distortions in the nanoparticles. The first one is the low temperature used for the synthesis of the particles, which could lead to a much higher density of defects than in the bulk material obtained through high-temperature treatments. The second possible reason is more intrinsically related to the small size of the particles, since it has been shown in other systems that the size reduction down to the nanometer range leads to distortions of their crystal lattice due to the increasing effect of the surface.[25]

A distinction between these two reasons may be made if the crystallinity of the particles can be improved while their small size is preserved. Postsynthesis improvement of the crystallinity of nanoparticles can only be achieved through thermal treatments of annealing. In the colloidal state, a common procedure consists of a hydrothermal treatment under limited conditions of temperature and pressure. We found that the size of our particles could be preserved only for hydrothermal treatments performed under relatively soft conditions (typically 130 °C for 10 h). Investigation of the emission properties of the resulting particles did not reveal any significant change compared to those of the initial particles so that no clear conclusions could be drawn.[7]

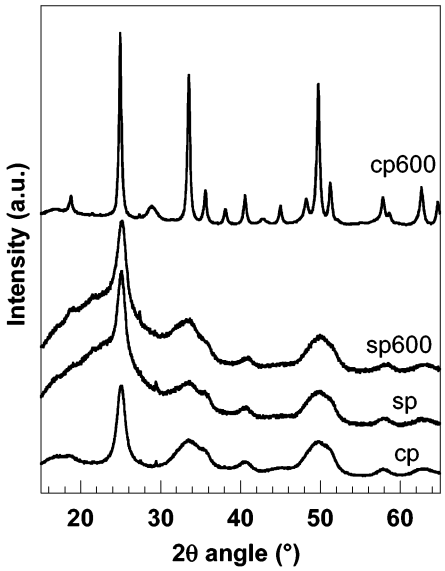

Figure 5. X-ray diffraction diagrams (Cu Kα) for both YVO_4:Eu (5% Eu^{3+}) crude and silica-capped nanoparticles after annealing at 600 °C. The large band observed in the 20−30° 2θ range for sp samples corresponds to the silicate shell.

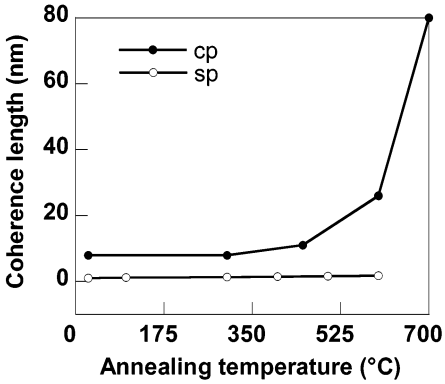

Figure 6. Evolution of the coherence length as a function of the annealing temperature for both YVO_4:Eu (5% Eu^{3+}) crude (cp) and silica-capped (sp) nanoparticles after annealing at 600 °C.

Further investigations were then performed on powders of nanoparticles treated at different temperatures up to 1000 °C. To discriminate the effect of thermal annealing and growth of the particles probably occurring at such a high temperature, both crude and silicated nanoparticles were studied. The evolution of the powder diffraction diagrams for different temperatures of annealing (Figure 5) shows that the increase of the coherence length begins at about 400 °C for crude particles, while no change can be measured in the case of silicated particles up to 600 °C (Figure 6). Note that, in this latter case, the investigations were limited at 600 °C because higher temperature treatments lead to the formation of an yttrium silicate phase.

The emission spectra of the nanoparticles (crude and silicated) as a function of their annealing treatments are presented in Figure 7. No evolution is observed in the case of the silicated particles for temperatures as high as 600 °C, in contrast with the behavior of the crude particles whose emission spectra progressively change from 400 °C, until they fit almost exactly the emission spectra of the bulk material. This result shows that the increase of the coherence length of the crude particles leads to the release of their structural distortions. This is confirmed by the Williamson−Hall analysis of the diffraction diagrams of the crude particles treated at 450 and 600 °C (Figure 8). Almost all lattice strains have disappeared at 600 °C, while the

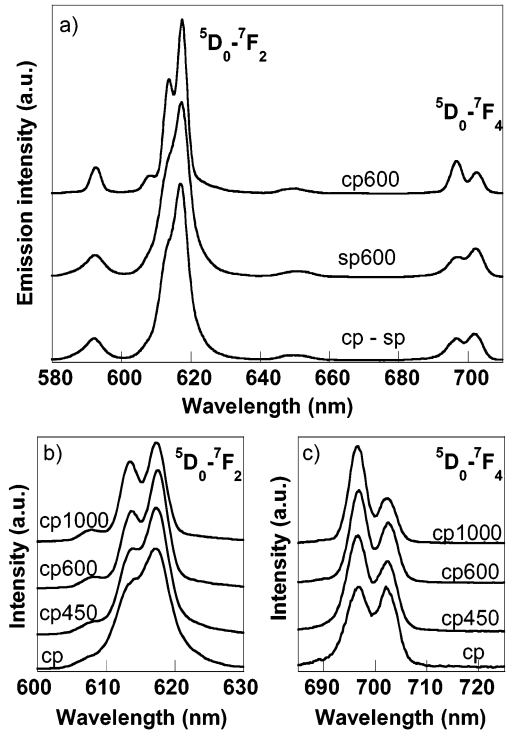

Figure 7. (a) Emission spectra for YVO_4:Eu (5% Eu^{3+}) crude and silica-capped nanoparticles after annealing at 600 °C. (b) and (c) show the temperature dependence of the $^5D_0-^7F_2$ and $^5D_0-^7F_4$ transitions, respectively.

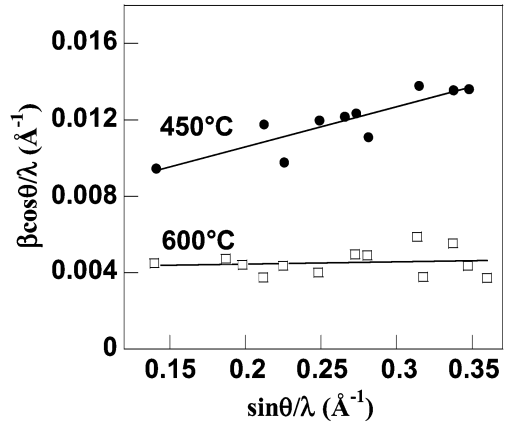

Figure 8. Size-strain analysis of X-ray diffraction patterns (Williamson−Hall plot) for crude nanoparticles heated at 450 and 600 °C. The intercept is the inverse of the crystallite size (11 and 24 nm at 450 and 600 °C, respectively). A nonzero slope indicates that strains are still appreciable within the sample heated at 450 °C. The slope tends to zero at 600 °C corresponding to a disappearance of distortions in nanoparticles.

crystallite size of the particles has increased from 11 to 24 nm. Such an analysis is not possible in the case of nonthermally treated particles because diffraction peaks are too large. However, the observed evolution of the crude particles between 450 and 600 °C is a clear indication that these particles present even more lattice strains than the sample treated at 450 °C. Since the diffraction diagrams of the silicated nanoparticles remain the same from ambient temperature up to 600 °C, we may conclude that the silicate shell prevents the removal of the distortions during the annealing treatments. This can be either a consequence of the impossibility for the particles to grow or because the lattice strains are related to defects which are anchored to the surface through the silicate shell. Both experiments clearly show that these distortions are closely related to the surface of the nanoparticles, and are thus a consequence of their small size. It is interesting to note that the crystallite size for which the distortions are released in the crude nanoparticles is 24 nm. This result is in good agreement with the emission properties of the YVO_4:Eu nanoparticles synthesized by Haase, which exhibit almost the same emission spectrum as the bulk material for a particle size between 15 and 18 nm.[8]

Structural Distortions: Influence on Luminescence Properties. We may now consider the influence of these thermal treatments on the emission efficiency. Figure 3 presents the evolution of the quantum yield of both crude (cp600) and silicated (sp600) particles treated at 600 °C as a function of their europium content.

In both cases, a global improvement of the luminescence efficiency is obtained through thermal treatments, but differences are observed between the silicated and crude particles. Concerning the annealed crude particles, the optimum quantum yield now reaches 40% while the $^5D_0$ lifetime has increased to 1.45 ms. This attests a decrease of the nonradiative quenching of the europium emission, due to the thermal removal of surface quenchers such as OH groups as confirmed by a thermogravimetric analysis. The same observation is made for annealed silicated particles, but the efficiency of this passivation seems to be enhanced. In this case, the optimum emission quantum yield now reaches 52% while the $^5D_0$ lifetime increases up to 1.7 ms. This better passivation compared to that of crude particles may be explained by the ability of the silicate shell to react with residual OH groups through hydrolysis/condensation reactions.

Concerning the optimum europium content, a clear decrease is observed for annealed crude particles so that the optimum is now similar to the bulk value (5%). No significant change of the optimum Eu content is observed after annealing of silicated particles. This shows that most of the possible passivation of the vanadates is already achieved by the silica-capping process at low temperature. These experiments tend to prove that energy migration processes are mainly affected by the quenching of the vanadate at the surface of the particles. In silicated particles, the passivation is mainly achieved through the chemical treatment of the surface. In crude particles, the annealing experiment cannot reveal whether the decrease of the vanadate quenching is only a consequence of the particle growth, which decreases the probability of surface quenching, or whether a thermally induced passivation mechanism of the surface should also be taken into account.

Concerning the effect of distortions, our experiments do not give clear indications that they may affect the energy migration processes. We may just infer that if there is an effect, it will be negligible since it could only explain the slight difference of the europium optimum concentration between the silicated and the crude particles annealed at 600 °C. Therefore, concerning energy transfers, the efficiency of distortion effects is much less important than the quenching of vanadate and europium at the surface of the particles.

Finally, the last point which can be discussed from this annealing experiment concerns the lifetime of the $^5D_0$ emission. Once most of the quenching species have been removed from the surface through thermal annealing at 600 °C, the radiative lifetime of both crude and silicated nanoparticles annealed at 600 °C is almost more than 1 ms higher than in the bulk material (Figure 4). A progressive transition toward the bulk behavior only occurs at 600 °C, and the bulk value is reached only after thermal treatments superior to 1000 °C. The most probable

explanation for this evolution must be found by considering the refractive index of the surrounding medium of the nanoparticles. It has indeed been shown in several systems that the radiative lifetimes of emission are strongly dependent on the refractive index of the immersion media.[11,26,27] This effect is of particular importance in the case of oxide nanoparticles, since the refractive index of the dispersions is usually much lower than that of the bulk material. This leads to an important increase of the radiative lifetime, which depends mainly on the refractive index of the surrounding media and the volume fraction of nanoparticles. Clear evidence for such effects has been obtained in the case of Y_2O_3:Eu nanoparticles dispersed in different media.[26] Our attempt to achieve the same experiments on vanadate nanoparticles did not succeed, mainly because nonradiative deexcitations in our systems are probably more important than those reported for Y_2O_3 nanoparticles. Then, it is not possible to claim that the decrease of lifetime observed by transferring the particles into a solvent with a higher index of refraction is not simply an effect of nonradiative relaxation. As a result, the observed decrease of lifetime occurring for thermal annealing of the crude powders at temperatures higher than 600 °C may indeed be explained by a progressive increase of refractive index due to the sintering of the powders. Nevertheless, other effects can contribute to this evolution of the radiative lifetime, among which is an increase of the emission cross section resulting from the release of internal strains within the crystalline lattice.

4. Conclusion

The luminescence properties of colloidal YVO_4:Eu nanoparticles (8 nm in diameter) are investigated and compared to those of the bulk materials. Differences are observed concerning the luminescence quantum yield and the $^5D_0$ emission lifetime as well as the optimum europium concentration. Chemical treatments were achieved to explain these differences. Improvement of the emission quantum yield after the transfer of the colloidal particles into D_2O shows that surface OH groups act as efficient quenchers of the Eu^{3+} emission. The growth of a silicate shell around the particles decreases the optimum europium concentration, showing that energy transfers within the nanoparticles are limited by the quenching of the excited states of the vanadate groups. Finally, high-temperature treatments were achieved to understand the impact of distortions on the energy-transfer processes within the nanoparticles. Experiments achieved on both crude and silicated powders of nanoparticles show that these distortions are directly related to the small size of the particles, probably through the high influence of their surface. Nevertheless, no clear evidence could be found concerning the influence of these distortions on the energy-transfer processes, since improvement of the emission properties as a function of the annealing treatments seems to result mostly from the elimination of Eu^{3+} and vanadate quenchers from the surface. This latter effect is greatly enhanced in the presence of the silicate shell compared to bare particles.

Acknowledgment. This work has been partially supported by Rhodia Electronics and Catalysis.

References and Notes

(1) Jüstel, T.; Nikol, H.; Ronda, C. *Angew. Chem., Int. Ed.* **1998**, *37*, 3085.

(2) Peng, X.; Schlamp, M. C.; Kadavanich, A. V.; Alivisatos, A. P. *J. Am. Chem. Soc.* **1997**, *119*, 7019. Counio, G.; Gacoin, T.; Boilot, J.-P. *J. Phys. Chem. B* **1998**, *102*, 5257.

(3) Blasse, G.; Grabmaier, B. C. *Luminescent materials*; Springer-Verlag: New York, 1994.

(4) Williams, D. K.; Yuan, H.; Tissue, B. M. *J. Lumin.* **1999**, *83*−*84*, 297. Li, Q.; Yan, D. *Nanostruct. Mater.* **1997**, *8(7)*. Schechel, R.; Kennedy, M.; Von Seggern, H.; Winkler, H.; Kolbe, M.; Fisher, R. A.; Xaomao, L.; Benker, A.; Winterer, M.; Hahan, H. *J. Appl. Phys.* **2001**, *89(3)*, 1679. Igarashi, T.; Ihara, M.; Kusunoki, T.; Ohno, K.; Isobe, T.; Senna, M. *Appl. Phys. Lett.* **2000**, *76(12)*, 1549. Dhanaraj, J.; Jagannathan R.; Kutty, T. R. N.; Lu, C.-H. *J. Phys. Chem. B* **2001**, *105(45)*, 11098.

(5) Zhang, W.; Xie, P.; Duan, C.; Yan, K.; Yin, M.; Lou, L.; Xia, S.; Krupa, J.-C. *Chem. Phys. Lett.* **1998**, *292*, 133.

(6) Murase, N.; Jagannathan, R.; Kanematsu, Y.; Kawasaki, Y.; Tomita, A.; Yazawa, T.; Kushida, T. *J. Lumin.* **2000**, *87*−*89*, 488.

(7) Huignard, A.; Gacoin, T.; Boilot, J.-P. *Chem. Mater.* **2000**, *12(4)*, 1090. Huignard, A.; Buissette, V.; Laurent, G.; Gacoin, T.; Boilot, J.-P. *Chem. Mater.* **2002**, *14*, 2264.

(8) Rivotzki, K.; Haase, M. *J. Phys. Chem. B* **1998**, *102*, 10129.

(9) Meyssamy, H.; Rivotzki, K.; Kornowski, A.; Naused, S.; Haase, M. *Adv. Mater.* **1999**, *11(10)*, 840.

(10) Riwotzki, K.; Meyssamy, H.; Kornowski, A.; Haase M. *J. Phys. Chem. B* **2000**, *104*, 2824.

(11) Stouwdam, J. W.; Van Heggel, F. C. J. M. *Nano Lett.* **2002**, *2(7)*, 733.

(12) Philipse, A. P.; Nechifor, A.; Pathmamanoharan, C. *Langmuir* **1991**, *10*, 4451.

(13) Huignard, A.; Gacoin, T.; Chaput, F.; Boilot, J.-P.; Aschehoug, P.; Viana, B. *Mater. Res. Soc. Proc.* **2001**, *667*, G4.5.

(14) Langford, J. I.; Louër, D. *Powder Diffr.* **1986**, *1(3)*, 211.

(15) Yu, M.; Lin, J.; Wang, Z.; Fu, J.; Wang, S.; Zhang, H. J.; Han, Y. C. *Chem. Mater.* **2002**, *14(5)*, 2224.

(16) Powell, R. C.; Blasse, G. Energy transfer in concentrated materials. *Structure and bonding*; Springer-Verlag: New York, 1980; Vol. 42.

(17) Blasse, G.; Bril, A. *Philips Tech. Rev.* **1970**, *31(10)*, 304.

(18) Ropp, R. C. *J. Electrochem. Soc. Solid State Sci.* **1968**, *115(9)*, 940; *Luminescence and the Solid State*; Elsevier: Amsterdam, 1951.

(19) Haas, Y.; Stein, G. *J. Phys. Chem.* **1972**, *76*, 1093.

(20) Riwotzki, K.; Haase, M. *J. Phys. Chem. B* **2001**, *105(51)*, 12709.

(21) Van Uitert, L. G.; Johnson, L. F. *J. Chem. Phys.* **1966**, *44(9)*, 3514.

(22) Blasse, G. *J. Chem. Phys.* **1966**, *45(7)*.

(23) Hernandez, R.; Franville, A.-C.; Minoofar, P.; Dunn, B.; Zink, J. I. *J. Am. Chem. Soc.* **2001**, *123*, 1248.

(24) Brecher, C.; Samelson, H.; Lempicki, A.; Riley, R.; Peters, T. *Phys. Rev.* **1967**, *155(2)*, 178.

(25) Li, Q.; Gao, L.; Yan, D. *Nanostruct. Mater.* **1997**, *8(7)*, 825. Nogami, M.; Nagasaka, K.; Kotani, K. *J. Non-Cryst. Solids* **1990**, *126*, 87. Counio, G.; Esnouf, S.; Gacoin, T.; Boilot, J.-P. *J. Phys. Chem.* **1996**, *100-(51)*, 20021.

(26) Lamouche, G.; Lavallard, P.; Gacoin, T. *Phys. Rev. A* **1999**, *59(6)*, 4668.

(27) Meltzer, R. S.; Feofilov, S. P.; Tissue, B.; Yuan, H. B. *Phys. Rev. B* **1999**, *60(20)*, R14012.